Collisionless shock and supernova remnant simulations on VULCAN

N. C. Woolsey, Y. Abou Ali, R. G. Evans, R. A. D. Grundy, S. J. Pestehe et al.

Citation: Phys. Plasmas **8**, 2439 (2001); doi: 10.1063/1.1351831
View online: http://dx.doi.org/10.1063/1.1351831
View Table of Contents: http://pop.aip.org/resource/1/PHPAEN/v8/i5
Published by the American Institute of Physics.

Collisionless shock and supernova remnant simulations on VULCAN*

N. C. Woolsey,† Y. Abou Ali, R. G. Evans, R. A. D. Grundy, and S. J. Pestehe
Department of Physics, Heslington, University of York, YO10 5DD, United Kingdom

P. G. Carolan, N. J. Conway, R. O. Dendy, P. Helander, and K. G. McClements
UKAEA Fusion, Culham Science Centre, Abingdon, OX14 3DB, United Kingdom

J. G. Kirk
Max-Planck-Institut für Kernphysik, Postfach 10 39 80, 69027 Heidelberg, Germany

P. A. Norreys, M. M. Notley, and S. J. Rose
Central Laser Facility, CLRC Rutherford Appleton Laboratory, Chilton, OX11 0QX, United Kingdom

(Received 19 October 2000; accepted 5 January 2001)

The VULCAN [C. N. Danson *et al.*, Opt. Commun. **103**, 392 (1993)] laser at the UK Central Laser Facility is being used for laboratory-based simulations of collisionless shocks. By ensuring that key dimensionless parameters in the experiments have values similar to those of supernova remnants (SNRs), the hydrodynamics and magnetic field of the experiment are scaled to those of a SNR. This makes it possible to investigate experimentally the physics of collisionless magnetized shocks in such objects. The experiments are providing data against which to test current theory. Collisionless shock formation and the interaction of two counterpropagating colliding plasmas permeated by a strong magnetic field are discussed. © *2001 American Institute of Physics.*
[DOI: 10.1063/1.1351831]

I. INTRODUCTION

High-power laser experiments have been used to provide information on space and astrophysical processes, and to test complex models of these processes. The material covered in the reviews by Ripin *et al.*,[1] Rose,[2] Remington *et al.*,[3] and Takabe *et al.*[4] illustrates the diverse impact of laser–plasma experiments. Experiments have been used to study radiative[2] and hydrodynamic properties,[1,3,4] and plasma equations of state.[5] Laser–plasma results have been applied previously to the study of such diverse environments as active galactic nuclei[6] and the Earth's bow shock.[7] More recent applications include the hydrodynamics of supernovae,[8] supernova remnants (SNRs), and the collision of galactic clouds.[9] Such experiments are made possible by ensuring that certain key dimensionless parameters in the laser-produced plasmas have values similar to those of the space and astrophysical plasmas of interest. Through this scaling detailed simulations of space and astrophysical plasmas can be carried out in the laboratory. Furthermore, modeling aspects can be tested directly against experiment.

Current interest in the laboratory simulation of astrophysical phenomena originated with the work of Remington and colleagues.[3,8] Our experiments differ qualitatively from this pioneering work in that we focus on *collisionless* plasma physics in a magnetized environment. The experimental technique is based on magnetic field and plasma production by direct drive laser irradiation. The scaling requirements for laboratory simulations of collisionless shocks such as those occurring at the interface between a supernova remnant (SNR) and the interstellar medium (ISM) are described in Sec. II. The experimental details and results are reported in Secs. III and IV, respectively. In Sec. V the experimental results are discussed, and finally conclusions are drawn in Sec. VI. *Système International* (SI) units have been used with the exception of temperature, which is quoted in electronvolts (eV).

II. SCALING

In scaling from SNR parameters to experimental ones, the following considerations apply. First, the system must be collisionless: this requires that the ratio of the ion mean-free path (mfp) to a typical scale length ζ be greater than unity. Second, despite the absence of collisions, it should be possible to describe the system using a fluid model. This can be done if a magnetic field is present such that particle gyroradii are smaller than the system scale length.[10,11] Third, certain dimensionless plasma parameters must have similar values in the astrophysical object and the laboratory experiment. Ryutov and co-workers[10,11] noted that the ideal fluid (Euler) equations are invariant under the ''Euler transformation,'' which preserves the ratio Eu of characteristic fluid speed to sound speed. Connor and Taylor[12] identified several transformations that ensure invariance of the magnetized ideal fluid equations. As shown by Ryutov and co-workers,[11] one of these transformations, labeled ''E_2'' by Connor and Taylor, can be combined with the Euler transformation as follows:

$$\mathbf{r}=a\mathbf{r}_1, \quad \rho=b\rho_1, \quad p=cp_1, \quad t=a(b/c)^{1/2}t_1,$$
$$\mathbf{v}=(c/b)^{1/2}\mathbf{v}_1, \quad \mathbf{B}=c^{1/2}\mathbf{B}_1, \tag{1}$$

where $\mathbf{r}$, t, $\mathbf{v}$, ρ, p, $\mathbf{B}$ denote, respectively, space, time, velocity, density, pressure, magnetic field, the transformed sys-

*Paper CI1 3, Bull. Am. Phys. Soc. **45**, 58 (2000).
†Invited speaker.

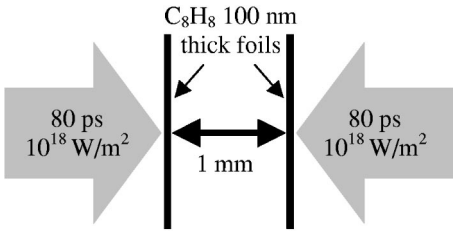

FIG. 1. Outline of the computational and experimental geometry, showing two 100 nm Å thick plastic foils separated by 1 mm. Lasers irradiated the two foils at 10^{18} W/cm^2 in an 80 ps pulse, as shown.

tem is labeled by the subscript ''1,'' and *a, b, c* are constants. It is apparent from Eq. (1) that both the Euler number Eu $=v(\rho/p)^{1/2}$ and the plasma beta $\beta=2\mu_0 p/B^2$ are invariant under the transformation. Thus, the role of the magnetic field at a supernova remnant can be simulated in the laboratory by matching the astrophysical β to the laboratory β. It is also necessary to ensure that a strong shock is formed: if the bulk fluid speed is U_f this requires that either the Alfvénic Mach number $M_A=U_f(\mu_0\rho)^{1/2}/B$ or the sonic Mach number $M \approx U_f(\rho/p)^{1/2}$ be greater than unity, depending on the value of β.

The one-dimensional laser–plasma fluid code MED103[13] was used to design the experiment. Using MED103 and the scaling considerations outlined above, a number of experimental configurations were explored. The experimental geometry was determined by the parameters of a SNR impacting the ISM 3×10^9 s (100 years) after the supernova explosion, scaled in accordance with Eq. (1), and by a consideration of VULCAN[14] energy limitations, including the need for a planar experiment amenable to detailed measurement. VULCAN is a 2.5 kJ, 8-beam Nd:Glass system with an operating wavelength of 1.053 μm, based at the Rutherford Appleton Laboratory in the UK.

The experimental geometry is shown in Fig. 1; similar experimental configurations have been used to study the interaction of two opposing supersonic plasmas created by laser ablation of a thick slab targets,[15] and opposing laser-exploded thin foils.[16,17] More recently,[9] radiatively heated thin foils were used to simulate hydrodynamic aspects of interstellar cloud collisions. All these experiments are collisional, compared to the experiment shown in Fig. 1, due to the high atomic number ($Z>6$), the high plasma densities ($n_e>10^{26}$ m^{-3}) and low plasma flow velocities ($<10^6$ m/s). Attempts to simulate this type of experiment have used one-dimensional multifluid simulations with interpenetrating computational grids coupled by an ion–ion collision parameter.[18] Alternative approaches use kinetic methods with collisions treated as binary Coulomb collisions using the Fokker–Planck approach,[19] or hybrid fluid electrons and particle ions models that incorporate collisions through Monte Carlo techniques.[20]

The experiments and simulated experiment depicted in Fig. 1 use two 100 nm thick C_8H_8 plastic foils placed face parallel and separated by 1 mm. The foils are irradiated simultaneously by lasers approaching from the left of the left-hand foil and from the right of the right-hand foil. Each foil

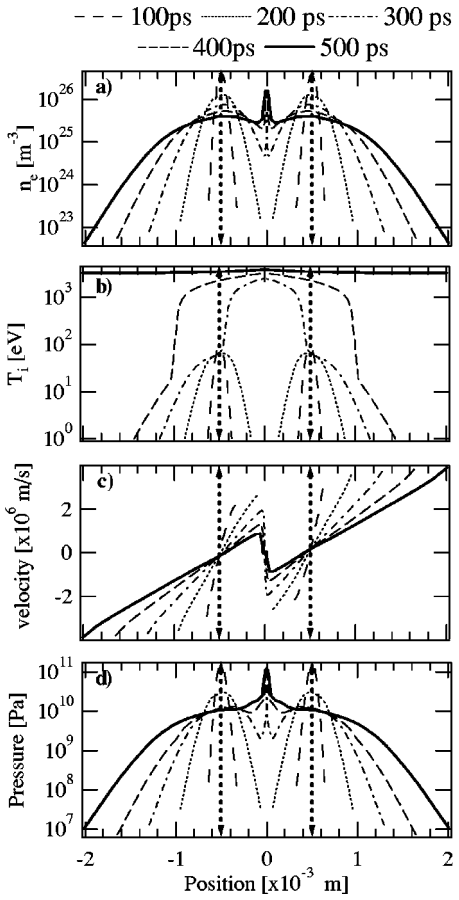

FIG. 2. MED103 simulation of the colliding foils experiment. These are fluid calculations and do not model the interpenetration as the plasmas collide at position 0 cm. The arrowhead lines indicate the initial positions of the foils. Electron density (a), thermal ion temperature (b), velocity (c), and pressure (d) are shown at 100 ps intervals.

is irradiated with a peak intensity of 10^{18} W/m^2 in 80 ps Gaussian laser pulses. The MED103 hydrodynamics model is used to predict the evolution of the plasmas. In Figs. 2(a) the electron density n_e, 2(b) the ion temperature T_i, 2(c) the fluid velocity U_f, and 2(d) pressure p, at 100 ps intervals are shown. The vertical arrowhead lines indicate the initial foil positions (placed at $\pm5\times10^{-4}$ m). On laser irradiating the foils, the foils explode and stream toward each other impacting at the midpoint: this is at 0 m in the figures, and occurs approximately 350 ps after the peak of the laser pulse. After 350 ps a central peak in n_e arises as two shocks form between the interface of the flowing and stagnating plasma. The n_e of the shocked region increases in time as material continues to stagnate. The regions on both sides of the central peak are referred to as the ''upstream,'' and the region of shocked or stagnated material (centred at 0 cm) is referred to as the ''downstream.'' This simulation provides numerical data for a comparison with parameters believed to be typical of SNRs 100 years after the supernova explosion. However, MED103 is a fluid model that accurately predicts the hydrodynamic expansion of the exploding foils but will *not* simulate the interpenetration of counterflowing plasmas. MED103 assumes the plasmas are collisional. In this case, we believe the simulation data for the experiment ''upstream'' are accu-

TABLE I. Both the SNR and upstream-simulated experiment at 500 ps are collisionless, as indicated by the collisionality parameter ζ, which is greater than unity. Electron density is denoted by n_e, the ion–ion mean-free path by λ_{ii}, the Debye length λ_{Debye}, and the size of the system by L. The upstream ion temperature T_i is calculated from the flow velocity.

	n_e (m^{-3})	T_i (eV)	L (m)	λ_{ii} (m)	λ_{Debye} (m)	$\zeta=\lambda_{ii}/L$
SNR	10^6	10	3×10^{16}	8×10^{11}	2.3×10^{3}	3×10^{4}
Sim U	3×10^{25}	5×10^{4}	5×10^{-4}	0.03	4.3×10^{-8}	56
Sim D	1×10^{26}	3850	5×10^{-5}	5×10^{-5}	4.7×10^{-8}	1

TABLE III. The hydrodynamic equivalence of a SNR and experiment is achieved by matching the Euler number, Eu. Typical values of a SNR are matched to the experiment upstream at 500 ps. v is a characteristic velocity, t characteristic time (i.e., age of system), ρ the density, and p the pressure.

	v (m/s)	ρ (kg/m^3)	p (Pa)	t (s)	Eu
SNR	10^7	10^{-21}	10^{-4}	3×10^{9}	3.1
Sim U	9×10^{5}	8×10^{-2}	1×10^{10}	5×10^{-10}	2.8
Sim D	2×10^{5}	0.5	1×10^{11}	1×10^{-10}	1

rate, whereas the simulation data ''downstream'' of the experiment are much more speculative.

Numerical parameters that satisfy approximately the scaling constraints described earlier are recorded in Tables I–IV. Characteristic values for a SNR at 100 years after the explosion of the supernova are compared to the simulated experiment; the experiment is designed to ensure the simulation at 500 ps matches the SNR at 100 years. The key dimensionless parameters used in the scaling are the following: in Table I the collisionality ζ, in Table II the plasma β (which is required to ensure the plasma is *effectively* collisional), in Table III the Euler number Eu, and in Table IV the Mach number M. The scaling parameters are shown in the right-hand columns. The upstream plasma is labeled Sim *U* in Tables I–IV, and the downstream plasma, labeled Sim *D*, is given for reference. An average atomic number of 3.5 and average atomic mass of 6.5 are used for the CH plasma.

The values of ζ recorded in Table I show that typical particle mean-free paths in a SNR are much larger than the associated scale lengths: the plasma is thus collisionless. Such large values of ζ cannot be matched in the laboratory. However, it is possible to ensure that the ion mean-free paths exceed experimental scale lengths by creating plasmas with high ion velocities and low n_e. An exploding foil is an ideal method to achieve high ζ: at 500 ps ζ is greater than unity, indicating that the plasma is collisionless.

In scaling the magnetic and hydrodynamic parameters, the SNR is described by (L, ρ, p, τ, B) and the experiment by (L_1, ρ_1, p_1, τ_1, B_1), where L is a characteristic scale length and τ is a characteristic time. The magnetic scaling is summarized in Table II and is determined by invariance of the plasma beta β. If $\beta\gg1$ the magnetic field pressure does not affect the hydrodynamics of the plasma: in a SNR $\beta\sim400$ is a possible value. Although the plasma beta may be large, the magnetic field can still give rise to an ''effective'' collisionality, in a SNR the ion gyroradius radius is small compared to typical scale lengths. Typical ISM magnetic fields are extremely small by laboratory standards, as shown in Table II, but are nevertheless believed to be strong enough to play an important role in collisionless shock formation. To achieve the correct scaling in the laboratory, large magnetic fields of order 20 T must be generated. The experiment is scaled to reproduce the same upstream plasma β through the scaling $\beta=\beta_1$. The role of the ISM magnetic field is simulated by the laboratory magnetic field. The parameters in Tables I and II indicate that the SNR plasma can be described by a fluid model since the ion r_i and electron r_e gryoradii are much smaller than the system size L (cf. Tables I and II). In the case of the exploding foil plasmas, the ratio L/r_e is much larger than unity, and the fluid approximation can be applied, while L/r_i is comparable to unity and so the application of a fluid model to the ions is less well justified. The small Debye radius (cf. Table I) ensures the ions do not break away from the electrons, thus the fluid approximation can be applied to the experiment with some justification.

The hydrodynamic scaling from the SNR to the laboratory involves changes in the values of physical parameters by factors of up to 10^{20}. The work of Ryutov and co-workers[10,11] demonstrates that magnetohydrodynamic equivalence can be rigorously achieved across such enormous changes in scale if the value of the Euler number and plasma β in the SNR are matched in the laboratory and if the Euler equations can be applied. The Euler number is given in terms of length and time scales by $\mathrm{Eu}=L(\rho/p)^{1/2}/\tau=L_1(\rho_1/p_1)^{1/2}/\tau_1$: for a 100 year old SNR Eu$\approx$3. The parameters shown in Table III indicate that the experiment hydrodynamics at $t=500$ ps will be equivalent to those of the SNR 100 years after the explosion.

Shock formation can be achieved in principle using counterstreaming plasmas, as depicted in Fig. 1. Values extracted from the MED103 simulations are recorded in Table IV: these results must be used with caution, as the model assumes fluid-like plasma motion and does not include a magnetic field. However, comparing the simulation with the

TABLE II. Magnetic parameters of the experiment are scaled to values typical of a SNR by adjusting the magnetic field strength, B, to give the same β, the ratio of thermal to magnetic energy. Here $r_{i,e}$ are the ion and electron gyroradii, respectively.

	B (T)	r_i (m)	r_e (m)	β
SNR	1×10^{-10}	3.2×10^{6}	7.5×10^{4}	400
Sim U	20	8.3×10^{-4}	3.6×10^{-6}	400
Sim D	20	2.3×10^{-4}	9.2×10^{-6}	190

TABLE IV. Values of Mach number, M, indicate that the SNR is in the strong shock regime, and that the shocks in the upstream of the experiment at 500 ps are of intermediate strength. Here U_s is the shock speed, C_s the sound speed, and u_{A} the Alfvén velocity.

	U_s (m/s)	C_s (m/s)	u_{A} (m/s)	M
SNR	5×10^{6}	4×10^{4}	2×10^{3}	$\sim$100
Sim U	1×10^{6}	2×10^{5}	6×10^{4}	$\sim$5
Sim D	1×10^{6}	1×10^{6}	3×10^{4}	1

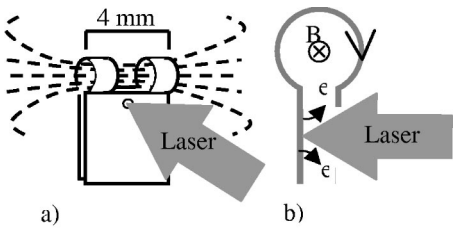

FIG. 3. Millimeter-scale Helmholtz coils (a) are used to create strong magnetic fields. A 1 μm wavelength laser at 10^{18} W/m^2 irradiates the back plate of the Helmholtz coil target to drive a hot electron source. The hot electrons generate a potential difference between the front and back plates and a return current in the Helmholtz coils results in the magnetic field. (b) shows a side view of the Helmholtz coil and the laser passing through a hole in the front plate.

SNR is instructive, and indicates that matching the SNR Mach number in the laboratory will be challenging. The simulated upstream plasma should generate intermediate strength sonic shocks compared with strong shocks observed in SNRs.

III. THE EXPERIMENT

The description of the experiment is divided into three parts: the creation of a magnetic field, the formation of collisionless plasmas, and the formation of a magnetized plasma. The principal experimental aim is to demonstrate the usefulness of laser systems similar to VULCAN for collisionless shock studies, and second, the scaling of these shocks to astrophysical phenomena such as supernova remnants. This requires the generation of large (tens of tesla) magnetic fields, and collisionless plasmas that could be immersed in this magnetic field.

The magnetic field was generated using ideas reported by Daido and co-workers.[21] In their work 60 T magnetic fields are generated with a CO_2 laser irradiating a single wire loop target at an intensity of 10^{18} W/m^2 and wavelength of 10 μm. In the experiments reported here, a single beam from a VULCAN laser, operating at 1.053 μm, was used to drive a novel mm-scale Helmholtz coil target. The Helmholtz coil design is shown in Fig. 3. This design offers the advantage of a uniform magnetic field in the region between the Helmholtz coils and space to incorporate additional targets (such as exploding foils), and also allows laser and diagnostic access. The Helmholtz coil consists of a photo-etched 50 μm thick copper sheet that is bent to form a 2.5 mm diam coil in the center with two parallel copper plates. A plastic insulating spacer, typically 500 μm thick, separates the copper plates. The Helmholtz coil is driven with 300 J contained in a 1 ns laser pulse, and focused to a 100 μm diam spot on the inner surface of the back plate [see Fig. 3(b)]. To allow laser access to the back plate, a hole was cut in the front plate and insulating plastic spacer with diameters of 0.5 and 1.2 mm, respectively.

We denote laser irradiance and wavelength by I and λ. At a peak $I\lambda^2$ of 10^{18} W/m^2 μm^2, similar to that used by Daido and co-workers,[21] a hot electron source with an approximate temperature of 15 keV is generated. The hot electrons preferentially stream down the electron density gradient formed as the copper target ablates, and stream toward the front copper plate. This causes a large potential difference between the back and front plates, which drives a reverse current. The reverse current flows through the Helmholtz coil to generate a magnetic field. As the critical density surface from the rear copper plate strikes the front plate a short circuit occurs. The reverse current circulates in the closed Helmholtz coil-plasma circuit with a decay determined by the impedance and resistance of the coil.

Two methods are employed to determine the magnetic field. The first of these involves the use of single-turn 1 mm diam search coils (induction coils), which are used coupled to a 1 GHz digital oscilloscope. Magnetic fields can be measured with and without a plasma between the Helmholtz coils. The second method involves the spectroscopic measurement of the ultraviolet (227 nm) carbon V (helium-like carbon) $1s2s^3S_1-1s2p^3P_{2,1,0}$ triplet transition. This technique is based on the measurement of any Zeeman splitting of the $J=2$ component: a polarizer is used to select only the σ-polarized components. This measurement requires a magnetic field to be present in the plasma. To ensure a high population of helium-like carbon, the exploding foils are replaced by a thick plastic slab, which is placed in the coil and ablated by the lasers.

Time- and space-resolved schlieren measurements are obtained of the counterstreaming exploding foil plasmas in the presence of a magnetic field. The schlieren diagnostic gives information on the spatial variation of refractive index across the probe beam. Since the refractive index is related to the electron density, the diagnostic can be used to determine electron density gradients perpendicular to the probe direction. The probe beam is directed normal to the plasma flow between the two exploding foils, as indicated in Fig. 4, and imaged past a stop placed at the focal spot, with the stop obstructing the unrefracted probe light. The focusing optics and stop size resulted in a diagnostic sensitive to densities above 5×10^{23} m^{-3}. Two-dimensional schlieren images with 80 ps time resolution, up to 1 ns during the evolution of the counterstreaming plasmas, are recorded.

Low-density ($<10^{24}$ m^{-3}), rapidly expanding, collisionless plasmas are formed by the explosion of CH foil targets. Two CH foils 100 nm thick, mounted on Mylar washers with a 1.2 mm diam hole, were positioned 1 mm apart. The foils were simultaneously illuminated over a 1 mm diam spot to ensure that each foil approximated a one-dimensional planar expansion. The large focal spots are achieved by defocusing the laser *or* using phase zone plates. The foils are irradiated with approximately Gaussian-shaped 80 ps pulses at 10^{18} W/m^2.

The schlieren measurements are the principal diagnostic for the exploding foils. Spatially resolved carbon K-shell x-ray spectroscopy complemented the schlieren measurement. The soft x-ray measurements used an imaging flat-field spectrometer with a 1200 lines/mm grating and Ni mirror coupled to a back-thinned 16-bit charged coupled device (CCD) detector filtered with 4 μm of Al. The spectrometer was configured to image the two exploding foils and the

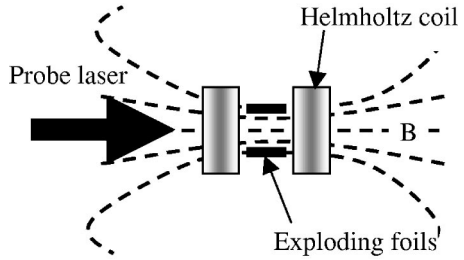

FIG. 4. The exploding foils can be positioned in the Helmholtz coils. This geometry is used in an attempt to magnetize the exploding plasmas. Values of plasma beta between 1 and several 100s are possible. There is significant uncertainty associated with the field penetration as the plasma expands.

region between them in one dimension and carbon K-shell spectra (between 3 and 4.5 nm) in the second dimension.

The magnetic field and the two foils were combined to attempt measurements of counterstreaming collisionless plasma in a magnetic field. Figure 4 shows the layout of the exploding foils and Helmholtz coils, and alignment of the schlieren probe. The exploding foil targets were positioned inside the Helmholtz coil targets, with the center point between the two foils placed in the center of the Helmholtz target. Accurate alignment is achieved using microscopes before inserting in the target chamber. When using the magnetic field the lasers are sequenced to ensure the magnetic field is generated before the foil targets are exploded. Typically, the Helmholtz coil is irradiated first, 2 ns later the plastic foils are exploded: the foils are probed approximately 500 ps later.

IV. RESULTS

The Helmholtz coils generated strong magnetic fields, with the search coil results indicating fields of the order of 40 T. The result is shown in Fig. 5, together with the integrated signal. The magnetic field decays with a time constant of 30 ns. This is in broad agreement with an estimated equivalent circuit impedance-resistance decay time of 20 ns. Using the Zeeman diagnostic, inconclusive observations were obtained of splitting of the carbon V $1s2s\ ^3S_1-1s2p\ ^3P_2$ component of the triplet: if interpreted as Zeeman splitting, this would indicate magnetic fields approaching 10 T. However, as only one time-integrated data shot was obtained this measurement must be treated with caution.

Schlieren images of the counterstreaming exploding foils are shown in Figs. 6 and 7. The position of the Helmholtz

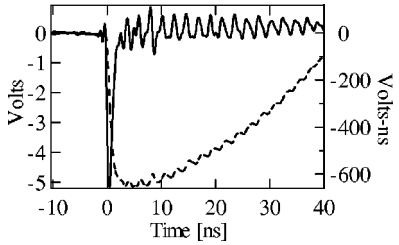

FIG. 5. Time-resolved search coil data (solid line) and the integrated signal (dashed line) indicate that magnetic fields of approximately 40 T were obtained.

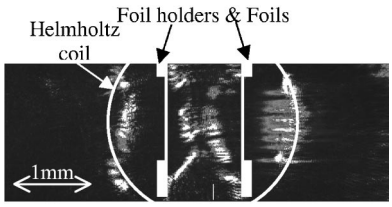

FIG. 6. The schlieren image of two exploding foils with *no* magnetic field. The foils are mounted inside a Helmholtz coil, with an image being taken 500 ps after peak of the laser. The positions of the foils and Helmholtz coil are indicated.

coil target, the two foil holders, and an initial position of the foils are shown. Both images are taken 500 ps after the peak of the laser pulse exploding the CH foil targets: Figure 6 shows a measurement with *no* magnetic field, Fig. 7 shows an experiment with similar laser irradiation conditions in the presence of a magnetic field. The images are similar. Recalling that schlieren data indicate regions of electron density gradient, we infer that the two edges of each of the exploding foil extend just beyond the Helmholtz coil and collide in the center of the figure. There are pronounced horizontal intensity modulations across the foils, indicating nonuniform electron density across the exploding plasmas. This structure is observed at all times that data was taken, i.e., with probe delays between 200 and 600 ps after the foils are exploded, without and with a magnetic field. The filamentation structure appears to be dependent on the focusing conditions as the structure scale length alters if the focusing conditions are changed. In Figs. 6 and 7 the filamentation scale length is approximately 100 μm and is observed across the 1 mm diameter laser focal spot. Vertical filaments in the bottom center of Fig. 7 are due to the plasma formed in the Helmholtz coil. This structure does not result from the exploding foils. The timing sequence in Fig. 7 ensured that the magnetic field was created 2 ns *before* the exploding plasmas were formed, whereas the exploding foils are probed 500 ps later. There are consistent differences between the schlieren images without (Fig. 6) and with (Fig. 7) a magnetic field present. Cross sections of the central region between the foil initial positions in Figs. 6 and 7 are compared in Fig. 8. The cross sections are averaged over 250 μm in the vertical direction. Schlieren images are consistently and reproducibly observed to be brighter in the presence of a magnetic field. A possible interpretation is that steeper electron density gradients occur when a magnetic field is present.

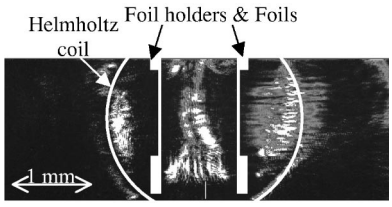

FIG. 7. The schlieren image of two exploding foils in a magnetic field. Image taken 500 ps after the peak of the laser. The positions of the foils and the Helmholtz coil are indicated.

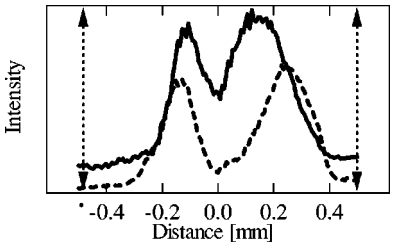

FIG. 8. Cross sections taken from the central region between the initial foil positions in Figs. 6 (dashed line) and 7 (solid line). Regions of higher schlieren intensity indicate steeper electron density gradients. The arrowhead lines indicate the initial positions of the foils.

V. DISCUSSION

The magnetic field generation was sufficient to achieve the magnetic scaling discussed in Sec. II, and the results confirm, as well as extend, the work of Daido and co-workers.[21] Our ultimate aim is to generate and use larger magnetic fields ($>100\,\mathrm{T}$): results we have obtained suggest that magnetic fields higher than 40 T can be created by shaping the leading edge of the laser pulse. This will ensure the peak laser irradiance is reached *before* the critical density surface reaches the front plate of the Helmholtz coil. This implies that stronger magnetic fields can be generated.

The Zeeman diagnostic produced inconclusive data: as such there is no experimental evidence of magnetic field penetration into the exploding foil plasmas (indeed the soft x-ray spectroscopy indicates that the exploding foil plasmas are hot and the population of helium-like carbon is low). Any magnetic field present in the foil before exploding will be attenuated by the factor of 10^4 expansion of the foil before collision. In addition, the plasma may exclude the free space magnetic field as it expands. Theoretical models based on ideal and resistive magnetohydrodynamics do not necessarily describe the complex plasma physics associated with the foils as the plasma density is low, the ion gyroradius approximates the experimental scale (see Table II), and the mean-free paths are long. However, schlieren results presented in Fig. 8 are reproducible, and when compared to hydrodynamic simulations of single foils imply the electron density gradients are steeper when a magnetic field is present. The schlieren method is sensitive only to the *magnitude* of the electron density gradient; it is not possible to state whether the electron density rises or falls as the two plasmas interact. Future electron density measurements will enable the sign of the electron density gradient to be determined.

There is no evidence that suggests the plasma will be decelerated due to the presence of a magnetic field. The planar expansion of the plasma suggest the magnetic field will be pushed aside as the plasmas converge, particularly as the low plasma density and high magnetic fields result in high Alfvén velocities; thus the plasma interfaces are not expected to be Rayleigh–Taylor unstable.

The schlieren imaging results have led to unexpected observations of density nonuniformities in rapidly expanding exploding foils. This density structure appears to have resulted from intensity nonuniformities across the laser focal spot. The laser imprint causes more rapid acceleration of regions of the exploding foil illuminated with an intensity hot spot than regions illuminated at a lower intensity. It is generally assumed that the effects of nonuniform laser illumination will be smoothed in the expanding plasma blowoff by the propagation of sound waves. Typically the effects of nonuniform illumination of solid laser targets have been of great concern, as nonuniform laser illumination is known to drive hydrodynamic instabilities. With a massive target the plasma blowoff produces an atmosphere that can smooth out nonuniform illumination in the later stages of the implosion, but the ''imprinting'' at early times remains a problem. Yet, low-density plasmas have received little attention. As an exploding foil expands rapidly efficient smoothing does not occur. Since the hydrodynamic expansion of these foils is supersonic (Mach number ~ 5) and planar the density modulations remain frozen in the plasma. Simple theoretical argument and two-dimensional hydrodynamic simulations support this conclusion.

VI. CONCLUSIONS

We have discussed experimental techniques required for the laboratory simulation of a collisionless shock, and, using scaling arguments, have demonstrated the relevance of such simulations to the investigation of a SNR impacting the ISM. Laboratory simulations of high Mach number collisionless shocks are of particular astrophysical importance, as such shocks are believed to be the primary acceleration sites for galactic cosmic rays with energies below $10^{15}\,\mathrm{eV}$. Fluid equations can be applied to SNR; in the experimental analog the ion gyroradius is large, however, the electron gyroradius and Debye length are small, so that the use of a fluid approximation is justified. The creation of counterstreaming collisionless plasmas is well within the operating capabilities of the VULCAN laser, and such experiments are ideal for detailed measurement. Our preliminary experiment has successfully demonstrated three essential requirements for the laboratory simulations. The first of these is the generation of a large magnetic field. This required the use and development of novel target geometry and methods. The use of a laser to generate the magnetic field enables the field to be synchronized to a laser–plasma experiment. Second, the creation of collisionless plasmas, as inferred from schlieren imaging of two counterstreaming exploding foils, has been achieved. Schlieren imaging measurements are sensitive to the magnitude of a density gradient *not* the sign of the gradient. The data indicate the density gradients between to the two plasmas are steeper when the magnetic field it present. However, without electron density measurements it is not possible to determine whether the gradient indicates a density spike or density depression at the midpoint between the plasmas. The experiment highlighted the need for uniform plasma production. Finally, a counterstreaming plasma experiment has been immersed in a strong magnetic field: available experimental results indicate that the magnetic field does not penetrate the plasma.

There is now an urgent need to address two key questions regarding the use of laser-irradiated plasmas for laboratory simulations of collisionless astrophysical plasmas.

First, the penetration of an external magnetic field into the plasmas; and second, the uniformity of the low-density plasma blowoff. We intend to pursue both issues as these experiments evolve. In summary, these experiments lie at the frontiers of laser–plasma interaction, and demonstrate that certain aspects of SNR physics can be recreated in the laboratory, thereby allowing the possibility of rigorously testing theoretical models of such objects.

ACKNOWLEDGMENTS

The authors wish to thank the Target Preparation, VULCAN Laser, and VULCAN Target Area staff at the Central Laser Facility for their expertise and hard work. N.C.W. acknowledges productive discussions with Paul Drake.

This work was supported in part by the UK Engineering and Physical Sciences Research Council, a Central Laser Facility Direct Access experiment, CEC-ERB FMR XCT 980168, and the UK Department of Trade and Industry.

[1]B. H. Ripin, C. K. Manka, T. A. Peyser, E. A. McLean, J. A. Stamper, A. N. Mostovych, J. Grun, K. Kearney, J. R. Crawford, and J. D. Huba, Laser Part. Beams **8**, 183 (1990).
[2]S. J. Rose, Phys. World **7**, 56 (1994).
[3]B. A. Remington, D. Arnett, R. P. Drake, and H. Takabe, Science **248**, 1488 (1999).
[4]H. Takabe, H. Nagatomo, A. Sunahara, N. Ohnishi, A. I. Mahdy, Y. Yoda, S. Naruo, H. Azechi, H. Nishimura, and K. Mima, Plasma Phys. Controlled Fusion **41**, A75 (1999).
[5]R. Cauble, T. S. Perry, D. R. Bach, K. S. Budil, B. A. Hammel, G. W. Collins, D. M. Gold, J. Dunn, P. Celliers, L. B. DaSilva, M. E. Foord, R. J. Wallace, R. E. Stewart, and N. C. Woolsey, Phys. Rev. Lett. **80**, 1248 (1998).
[6]A. Levinson and R. Blandford, Mon. Not. R. Astron. Soc. **274**, 717 (1995).
[7]A. R. Bell, P. Choi, A. E. Dangor, O. Willi, D. A. Bassett, and C. J. Hooker, Phys. Rev. A **38**, 1363 (1988).
[8]B. A. Remington, R. P. Drake, H. Takabe, and D. Arnett, Phys. Plasmas **7**, 1641 (2000).
[9]T. S. Perry, R. I. Klein, D. R. Bach, K. S. Budil, R. Cauble, H. N. Kornblum, R. J. Wallace, and R. W. Lee, Astrophys. J., Suppl. **127**, 437 (2000).
[10]D. Ryutov, R. P. Drake, J. Kane, and B. A. Remington, Astrophys. J. **518**, 821 (1999).
[11]D. D. Ryutov, R. P. Drake, and B. A. Remington, Astrophys. J., Suppl. **127**, 465 (2000).
[12]J. W. Connor and J. B. Taylor, Nucl. Fusion **17**, 1047 (1977).
[13]A. Djaoui and S. J. Rose, J. Phys. B **25**, 2745 (1992).
[14]C. N. Danson, L. I. Barzanti, Z. Chang, A. E. Damerell, C. B. Edwards, S. Hancock, M. H. R. Hutchinson, M. H. Key, S. Luan, R. R. Mahadeo, I. P. Mercer, P. Norreys, D. A. Pepler, D. A. Rodkiss, I. N. Ross, M. A. Smith, R. A. Smith, P. Taday, W. T. Toner, K. W. M. Wigmore, T. B. Winstone, R. W. W. Wyatt, and F. Zhou, Opt. Commun. **103**, 392 (1993).
[15]R. L. Berger, J. R. Albritton, C. Randall, C. Hanna, W. L. Kruer, A. B. Langdon, and E. A. Williams, Phys. Fluids B **3**, 3 (1991).
[16]O. Rancu, P. Renaudin, C. Chenais-Popovics, H. Kawagashi, J. C. Gauthier, M. Dirksmoller, T. Missalla, L. Uschmann, E. Forster, O. Larroche, O. Peyrusse, O. Renner, E. Krousky, H. Pepin, and T. Shepard, Phys. Rev. Lett. **75**, 3854 (1995); C. Chenais-Popovics, P. Renaudin, O. Rancu, F. Gilleron, J. C. Gauthier, O. Larroche, O. Peyrusse, M. Dirksmoller, P. Sondhauss, T. Missalla, I. Uschmann, E. Forster, O. Renner, and E. Krousky, Phys. Plasmas **4**, 190 (1997).
[17]A. S. Wan, T. W. Barbee, R. Cauble, P. Celliers, L. B. DaSilva, J. C. Moreno, P. W. Rambo, G. F. Stone, J. E. Trebes, and F. Weber, Phys. Rev. E **55**, 6293 (1997).
[18]R. A. Bosch, R. L. Berger, B. H. Failor, N. D. Delamater, and R. L. Kauffman, Phys. Fluids B **4**, 979 (1992).
[19]O. Larroche, Phys. Fluids B **5**, 2816 (1993).
[20]P. W. Rambo and J. Denavit, Phys. Plasmas **1**, 4050 (1994); P. W. Rambo and R. J. Procassini, *ibid.* **2**, 3130 (1995).
[21]H. Daido, F. Miki, K. Mimi, F. Fujita, K. Sawai, K. Fujita, Y. Kitagawa, S. Nakai, and C. Yamanaka, Phys. Rev. Lett. **56**, 846 (1986).